Engineering Notes

ENGINEERING NOTES are short manuscripts describing new developments or important results of a preliminary nature. These Notes cannot exceed 6 manuscript pages and 3 figures; a page of text may be substituted for a figure and vice versa. After informal review by the editors, they may be published within a few months of the date of receipt. Style requirements are the same as for regular contributions (see inside back cover).

Flat Spin of Circular Cylinders Induced by Artificial Roughness

Takashi Yoshinaga,* Atsushi Tate,† and Kenji Inoue‡
National Aerospace Laboratory
Chofu, Tokyo, Japan

Nomenclature

C_D = drag coefficient of a circular cylinder for unit length
C_L = lift coefficient of a circular cylinder for unit length
C_n = yawing moment coefficient = moment $\times 8/(\rho V_\infty{}^2 d^2 r_0 \pi)$
D = drag force
d = diameter
L = lift force
l = length
N = steady rotation rate, Hz
Re = Reynolds number
r = distance from the axis of rotation, $\bar{r}=r/r_0, \Delta\bar{r}=\Delta r/r_0$,
r_m = mean distance, $\bar{r}_m = r_m/r_0$
r_0 = half length of the cylinder
V = velocity
θ = twisted angle of roughness elements (See Fig. 4)
η = calibration factor
ϕ = rotation rate, $\dot{\phi}_0 = 2\pi N r_0/V_\infty$

Subscripts

∞ = freestream
cr = critical
N = normal

Introduction

It has been reported that falling slender bodies with the center of gravity near their middle rotate in a plane normal to the freestream velocity (flat spin).[1] Wind tunnel experiments show that the high speed flat spin ($\sim$10 Hz) usually occurs near the critical Reynolds number Re_{cr}.[2] This suggests that the flat spin phenomena are closely related to the lift L ($C_L \cong 1$) acting on a circular cylinder at Re_{cr} where the boundary layer separates asymmetrically, since a bubble is formed on one side.[3,4] The steady rotation rate N (Hz) has been estimated with the quasi-two-dimensional assumption,[5] where the cross flow component is predominant over the cylinder. But the method failed to predict N for some cases; therefore, three-dimensionality should be included in the estimation. As a method to produce lift on a circular cylinder to simulate flat spin, the artificial transition of the boundary layer on one side is expected to be useful.

Submitted May 1, 1983; revision received Aug. 31, 1983.

*Head, Aerothermodynamics Section, First Aerodynamics Division. Member AIAA.
†Research Official, Aerothermodynamics Section, First Aerodynamics Division
‡Head, Boundary Layer Research Section, First Aerodynamics Division. Member AIAA.

The purpose of this note is to test if the artificial transition of a boundary layer over a cylinder could produce the moment of flat spin, and to examine how far the quasi-two-dimensional model is applicable to estimate N of the flat spin induced by the above method at $Re < Re_{cr}$.

Quasi-Two-Dimensional Analysis

We consider a two-dimensional cylinder on which lift owing to artificial asymmetric separation of the boundary layer is acting and which is allowed to move in a plane normal to V_∞ as in Fig. 1a. The cylinder moves right at V_L where the normal component of L balances with that of D. The V_L reduces to

$$V_L = V_\infty \cdot \tan\alpha = V_\infty \cdot C_L/C_D \tag{1}$$

If we assume that $C_L \cong 1$ and $C_D \cong 0.4$ as observed at Re_{cr},[3,4] it follows that $V_L \cong 2.5 \cdot V_\infty$. This suggests that a circular windmill could rotate at a high rate by the artificial boundary layer transition.

Figure 1b illustrates the quasi-two-dimensional estimation of the moment acting on a rotating circular cylinder. Integrating dL_N and dD_N acting on the elemental cylinder dr at r, C_n is expressed as

$$C_n(\dot{\phi}) = \frac{r_0}{d}\frac{4}{\pi}\int_{-1}^{1} \bar{r}(1+\dot{\phi}^2\bar{r}^2)^{1/2}(C_L - C_D\bar{r}\dot{\phi})\,d\bar{r} \tag{2}$$

The values of C_L and C_D are selected according to the result in the critical region: for the region without roughness, $C_D \cong 1$ and $C_L \cong 0$; for the region with roughness, $C_{D,cr} \cong 0.4$ and $C_{L,cr} \cong 1$. When $\bar{r}\dot{\phi} \ll 1$, we can estimate the integral on the right side of Eq. (2) by taking the first order terms of $\dot{\phi}$. The N is obtained as the root of $C_n(\dot{\phi}) = 0$. For a pair of narrow roughness strips of width $\Delta\bar{r} \ll 1$ stuck at $\pm\bar{r}_m$ symmetrically with respect to the axis of rotation, we have

$$N = \eta\,(3/2\pi)\bar{r}_m\Delta\bar{r}/r_0\,(C_{L,cr}/C_{D,cr})\,V_\infty \tag{3}$$

Models and the Apparatus

A small aluminum alloy model, 50 mm diam. and length 400 mm, was supported by a sting 6 mm diam. with ball bearings. The sting holder was fixed in the middle of a wind tunnel parallel to the freestream by steel wires of 0.5 mm diam. The cross-section of the closed return wind tunnel is 550×650 mm. A large model with 200 mm diam., in length 1040 mm, made of methacrylic acid resin, was supported by ball bearings and a sting. The sting holder was supported by 2 mm diam. steel wires in a larger wind tunnel with a cross-section of 2000×2000 mm. For roughness, sandpaper strips of grades 120, 100, 60, and 40, and twisted wires were used. The N was measured by counting the number of the pulses produced when the model crossed a He-Ne laser beam or the pluses produced by a rotary encoder.

Results and Discussion

Figure 2 shows the variation of N vs V_∞ for the small cylinder model with narrow sandpaper strips (10×50mm, 120 grade). Because the stagnation line might shift downstream

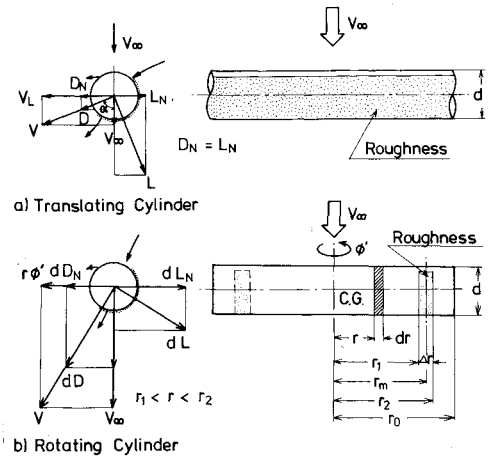

Fig. 1 Schematic diagram of elemental flowfield on circular cylinders.

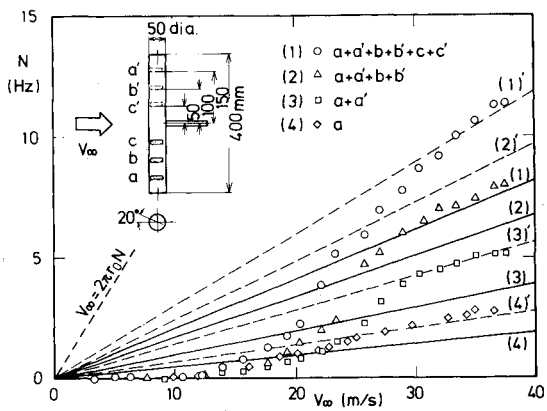

Fig. 2 Steady rotation rate of small cylinder with narrow sandpapers (10×50 mm, grade 120) vs V, (−), Eq. (2); (− − −). Eq. (2) effective roughness width is assumed as 1.4 times.

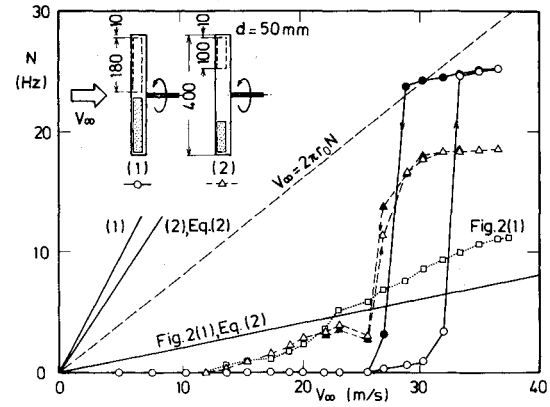

Fig. 3 Steady rotation rate N of small cylinder with wide sandpapers (180×50 mm and 100×30 mm, grade 120) vs V_∞. Solid symbols correspond to decreasing velocity.

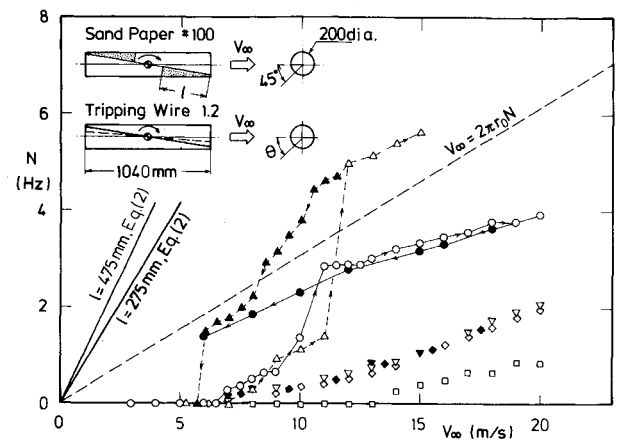

Fig. 4 Steady rotation rate N of large cylinder with roughness vs V_∞. (△) sandpaper 475×115 mm, grade 120; (○) sandpaper 275×115 mm; (□) 1.2 diam. wire with $\theta=22.5°$; (▽) 1.2 mm diam. wire with $\theta=45°$; (◇) 1.2 mm diam. wires with $\theta=22.5°$ and $\theta=4.5°$ at a time.

when the cylinder rotates, the sandpaper strips were also glued on three locations, covering from 20° to 130° downstream of the front generating line. The model began to rotate at $V_\infty \gtrsim 12$ m/s ($Re_\infty \gtrsim 4.2\times10^4$), and relations between N and V_∞ approached straight lines through the origin. On the other hand, according to the analysis, N is proportional to V_∞ as shown by solid lines. If we suppose that a fully turbulent boundary layer was produced beyond 30 m/s, the experimental data are partially understood. At $V_\infty \cong 30$ m/s ($Re_\infty \cong 10^5$), the experimental value is about 30 to 60% greater than the estimation, which cannot be calibrated even if we take $C_L \cong 1.2$ or 1.3.[3] As a tentative calibration, 1.4 times the width of the sandpaper is used in Eq. (2). When this is done, the variation of N approaches the experimental data for $V_\infty \gtrsim 30$ m/s. The difference in N for increasing and then decreasing V_∞ (hysteresis) is very little.

Figure 3 shows the variation of N vs V_∞ of a cylinder on which a pair of wide sandpaper strips were symmetrically glued 20° downstream from the front generating line. When 120 grade sandpaper, 180×50 mm was used, at $V_\infty = 32$ m/s the cylinder suddenly began to rotate at $N \cong 25$ Hz. When the wind velocity was decreased, the flat spin continued, i.e., the hysteresis of N similar to a natural transition (Ref. 2) was observed. With 120 grade sandpaper of 100×50 mm, the cylinder suddenly showed high speed rotation at $V_\infty = 26$ m/s, but little hysteresis was observed. The flow around the model seems to change to a different mode in the high-speed rotation. For wide roughness strips, the steady rotation rate is less than half of the rate predicted by the quasi-two-dimensional model. Though the nominal stagnation line might come on the roughness at a high rotation rate, this is not the main reason, as is shown by later experiments.

Figure 4 shows variation of N vs V_∞ for a large cylinder of 200 mm diam. Meshed stainless steel wires of 1.2 mm diam. were attached from end to end along the surface with twisted angles θ of 22.5° and 45°. The ratio of $2\pi r_0 N$ to V_∞ was small. For wires with $\theta=45°$, the N was greater than that for $\theta=22.5°$. When the two wires were tightened at the same time, the upstream wire had almost no effect on the rotation. Two pairs of 100 grade sandpaper strips of 475×115 mm and 275×115 mm with $\theta=45°$ were tested separately. In both cases, the rate N increased gradually up to $V_\infty \cong 10$ m/s, and then changed to higher rotation. The circumferential speed for the former reached about $1.3\cdot V_\infty$, but N was less than half of that predicted by Eq. (2), and hysteresis of N vs V_∞ also existed.

In addition, the following phenomena were observed with the large cylinder. When $\theta=22.5°$ and at large N, the normal stagnation line might be expected to appear on the sandpaper so that N would be smaller than for $\theta=45°$; for the grade 100 sandpaper, N is smaller for $\theta=22.5°$ than for $\theta=45°$; however, for grade 60, the situation was reversed. When ten sheets of sandpaper (40×115 mm, grade 60) were glued with $\theta=22.5°$ at 100 mm intervals, the rate was almost the same as for two sheets of continuous sandpaper (475×115 mm, grade 60) with $\theta=22.5°$, showing the increase of the effective area.

In conclusion, the experiments suggest that the rotation rate of the natural flat spin does not far exceed the order of $N \cong V_\infty/(2\pi r_0)$. Each sheet of narrow sandpaper on a circular

cylinder independently produces the moment and rotates the cylinder at a greater rate than predicted by the two-dimensional model. Wide sandpaper showed the hysteresis and jump of the N against V_∞, and the N was far less than that predicted by the quasi-two-dimensional model. The three-dimensional effect seems to be great.

References

[1]Research Group for Recovery of Sounding Rocket Payloads, "Investigation of High-Angle-of-Attack Aerodynamic Characteristics of a Payload of a Sounding Rocket for Material Processing Experiments III. On a Flat Spin in an Airdrop Test," NAL TM-426, Dec., 1980, National Aerospace Laboratory, Chofu, Tokyo, Japan. (in Japanese)

[2]Kubota, H., Arai, I., and Matsuzaka, M., "Flat Spin of Slender Bodies at High Angles of Attack," *Journal of Spacecraft and Rockets,* Vol. 20, Feb. 1983, pp. 108-114.

[3]Bearman, P. W., "On Vortex Shedding from a Circular Cylinder in the Critical Reynolds Number Regime," *Journal of Fluid Mechanics,* Vol. 37, July 1969, pp. 577-585.

[4]Kamiya, N., Suzuki, S., and Nishi, T., "On the Aerodynamic Force Acting on a Circular Cylinder in the Critical Range of the Reynolds Number," AIAA Paper 79-1475, July 1979.

[5]Yoshinaga, T., Tate, A., and Inoue, K., "Approximate Calculation of Aerodynamic Coefficients for Rotating Slender Bodies at 90 deg Incidence," *Journal of Spacecraft and Rockets,* Vol. 19, Jan. 1982, pp. 84-86.

Reynolds Number Effects on the Aerodynamics of a Body with Square Cross-Section

D. C. Daniel*
Air Force Armament Laboratory, Eglin AFB, Florida
and
G. J. Zollars† and T. R. Yechout†
United States Air Force Academy
Colorado Springs, Colorado

Introduction

RECENTLY, considerable attention has been given to Reynolds number effects on the flow separation about bodies of revolution at angle of attack. This research is perhaps best exemplified by the definitive work of Lamont,[1] which represents comprehensive results over a wide range of Reynolds numbers and angles of attack for a pointed ogive cylinder. Much attention has also been focused recently on the aerodynamic and flow separation characteristics of bodies that are noncircular in cross-section.[2-5] This Note brings together some of both groups of work by presenting experimental results which show the effects of Reynolds number on the normal force and rolling moment of a body that is square in cross-section. Results are presented for body-alone and body-fin configurations. The following paragraphs include a brief description of the wind tunnel facilities, models, and test conditions followed by a discussion of the results and some concluding remarks.

Submitted April 7, 1983; revision received July 21, 1983. This paper is declared a work of the U.S. Government and therefore is in the public domain.

*Chief, Aerodynamics Branch. Associate Fellow AIAA.

†Major, USAF, Assistant Professor of Aeronautics.

Facilities, Models, and Test Conditions

The experimental data presented in this Note were acquired in the subsonic and trisonic wind tunnels at the United States Air Force Academy.[6] The subsonic tunnel is a continuous flow, closed circuit facility with a test section of 2 × 3 ft. The trisonic tunnel is a blowdown facility with 1 × 1 ft test section.

Two wind tunnel models, both of the same design and differing only in scale, were used in this study. The primary model was a cylinder of square cross-section with a highly blunted ogival nose. The total body length was 7.5 in. The body cross-section width was 1 in. The cross-section corner radii were 0.2 in. A second model that was twice the size of the primary model was also used to acquire some of the data in the subsonic tunnel.

In addition to data for the body-alone configuration, data were also acquired for a body-fin arrangement. For these cases, the fins were arranged in a cruciform manner at the aftmost position on the body. The fins were attached at the body cross-section corners. At zero roll the fins were in an X configuration. The aspect ratio of the fins (based on exposed semi-span) was 0.47. A sketch of the body-fin model is shown in Fig. 1.

Six-component force and moment data were obtained for the angle-of-attack range 0 to 30 deg at roll angles of 0, 22.5, and 45 deg. Reynolds numbers (based on body cross-section width) varied from approximately $1.2 \cdot 10^5$ to $1.2 \cdot 10^6$. In order to obtain this range of Reynolds numbers, it was necessary to vary Mach number. Data required at Reynolds numbers of approximately $2.5 \cdot 10^5$ and below were taken at a Mach number of approximately 0.3, whereas the higher Reynolds number data were taken at a Mach number of 0.8. The effect of this subsonic Mach number variation will be discussed in the following section as required.

Results

Normal force and rolling moment results for the body-alone and body-fin configurations are shown in Figs. 2, 3, and 4. Figure 2 presents nonrolling, body-fixed, normal force coefficient variation with Reynolds number for both configurations at two roll orientations and at 26 deg angle of attack. Also presented in this figure for comparison are normal force data from Lamont's research on a pointed ogive circular cylinder.[1] Lamont determined that for the angle of attack shown (26°), separation was laminar for Reynolds numbers below approximately $2 \cdot 10^5$, transitional for Reynolds numbers between approximately $2 \cdot 10^5$ and 10^6, and turbulent above 10^6. As can be seen, the square body-alone results for the zero roll orientation follow the trend of Lamont's data, although the decrease in normal force as the Reynolds number increases is not nearly as pronounced. Likewise the recovery is not nearly as pronounced as the Reynolds number continues to increase. It should also be pointed out that the data points at the higher Reynolds numbers are probably slightly high (~10%) due to increased Mach number. This degree of increase with Mach number for square bodies has been documented by Schneider.[4]

Two data points are also shown on Fig. 2 for the body-alone case at a 45-deg roll orientation. Here the change in normal force is much more pronounced as the Reynolds number increases above $2 \cdot 10^5$. Unfortunately, no data were

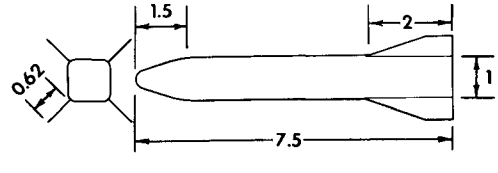

(Note: All dimensions in inches.)

Fig. 1 Body-fin wind tunnel model.